PART IV

Mechanical Stimuli to Cells

CHAPTER 19

Tools to Study Cell Mechanics and Mechanotransduction

Tanmay P. Lele,[⋆,1] Julia E. Sero,[⋆] Benjamin D. Matthews,[⋆,†] Sanjay Kumar,[⋆,2] Shannon Xia,[⋆] Martin Montoya-Zavala,[⋆] Thomas Polte,[⋆] Darryl Overby,[⋆,3] Ning Wang,[‡] and Donald E. Ingber[⋆]

[⋆]Vascular Biology Program
Departments of Pathology and Surgery
Children's Hospital and Harvard Medical School
Boston, Massachusetts 02115

[†]Department of Pediatrics
Massachusetts General Hospital and Harvard Medical School
Boston, Massachusetts 02114

[‡]Department of Mechanical Science and Engineering
University of Illinois at Urbana-Champaign
Urbana, Illinois 61801

[1] Department of Chemical Engineering, University of Florida, Gainesville, Florida 32611.
[2] Department of Bioengineering, University of California, Berkeley, Berkeley, California 94720.
[3] Department of Biomedical Engineering, Tulane University, New Orleans, Louisiana 70118.

METHODS IN CELL BIOLOGY, VOL. 83

0091-679X/07 $35.00
DOI: 10.1016/S0091-679X(07)83019-6

Abstract

Analysis of how cells sense and respond to mechanical stress has been limited by the availability of techniques that can apply controlled mechanical forces to living cells while simultaneously measuring changes in cell and molecular distortion, as well as alterations of intracellular biochemistry. We have confronted this challenge by developing new engineering methods to measure and manipulate the mechanical properties of cells and their internal cytoskeletal and nuclear frameworks, and by combining them with molecular cell biological techniques that rely on microscopic analysis and real-time optical readouts of biochemical signaling. In this chapter, we describe techniques like microcontact printing, magnetic twisting cytometry, and magnetic pulling cytometry that can be systematically used to study the molecular basis of cellular mechanotransduction.

I. Introduction

Cellular mechanotransduction refers to the processes by which cells convert physical forces into changes in intracellular biochemistry. These processes are critical for control of cell growth, migration, differentiation, and apoptosis during organogenesis and wound repair. Destabilization of cell and tissue structure, or dysfunctional mechanotransduction, can lead to the development of numerous diseases and debilitating conditions, including atherosclerosis, hypertension, asthma, osteoporosis, and cancer (Ingber, 2003a). Analysis of how cells sense and respond to mechanical stress has been limited by the availability of techniques that can apply controlled mechanical forces to living cells while simultaneously measuring changes in cell and molecular distortion, as well as alterations of intracellular biochemistry. We have confronted this challenge by developing new engineering methods to measure and manipulate the mechanical properties of cells and their internal cytoskeletal and nuclear frameworks, and by combining them with molecular cell biological techniques that rely on microscopic analysis and real-time optical readouts of biochemical signaling.

The methods we describe here emerged from systematic testing of an underlying hypothesis relating to cell structure, matrix mechanics, and mechanotransduction that has driven the work in our laboratory for over 25 years. Early views of the cell prior to the mid-1970s postulated a mechanical structure consisting primarily of an elastic membrane surrounding a viscoelastic cytoplasm (e.g., like a balloon filled with molasses or jello), and many engineering models of the cell are still based on

this vision (Dong and Sung, 1991). In contrast, we proposed that a cell uses a specific form of architecture known as "tensegrity" to structure its cytoskeleton, and that cells are composed of an interconnected network of tensed cables and membranes stabilized by compressed struts and substrate anchors (i.e., more like a tent than a water balloon) (Ingber, 1993a, 2003b; Ingber and Jamieson, 1985). This model predicts that contractile microfilaments and intermediate filaments in anchored cells function as cables which distribute tensile forces throughout the cytoplasm and nucleus, whereas compressive forces are resisted through cell adhesions by underlying extracellular matrix (ECM) and by neighboring cells, as well as by internal cytoskeletal struts such as microtubules or cross-linked actin bundles.

This view of cell structure led us to propose that transmembrane receptors such as integrins that physically integrate the cytoskeleton into the ECM may function as mechanoreceptors that provide a preferred path for mechanical force transfer across the cell surface (Ingber, 1991; Ingber and Jamieson, 1985). The cellular tensegrity model assumes that forces channeled through these discrete linkages become focused locally at the site of ECM anchorage within specialized cytoskeletal anchoring complexes known as "focal adhesions," and at distant sites throughout the cytoplasm and nucleus due to mechanical connectivity across discrete molecular linkages throughout the ECM–cytoskeleton–nuclear matrix lattice.

Importantly, many of the enzymes and substrates that mediate most of the cell's metabolic machinery perform their functions when physically immobilized on these macromolecular scaffolds (Ingber, 1993b). Thus, an important corollary to the tensegrity model of cell mechanics is that forces applied to cells and transmitted to the cytoskeleton through transmembrane integrin receptors may be converted into changes in intracellular biochemistry and gene expression at the nanometer scale through stress-dependent distortion of cytoskeletal-associated molecules (Ingber, 1997, 2006; Ingber and Jamieson, 1985). Force-induced changes in the shape of these load-bearing proteins will alter their chemical potential, thereby changing their kinetic and thermodynamic behavior, and hence, altering their biochemical activities.

If cells are structured using tensegrity, then cell shape stability will depend on a mechanical force balance between cytoskeletal traction forces and the ability of the ECM substrate to resist these stresses which will create a state of isometric tension, or a tensional "prestress" in the cytoskeleton and linked ECM. The tensegrity model therefore predicts that at the whole tissue level, changes in ECM mechanics may alter cell shape, cytoskeletal organization, and the steady state of mechanical balance, or prestress, inside the cytoskeleton, and that this, in turn, may alter intracellular biochemistry. This is important because it suggests that local variations in ECM structure and mechanics that are observed in developing tissues may contribute to the regional differentials in growth and motility that drive morphogenetic changes of tissue form in the embryo, as well as in certain disease processes (Huang and Ingber, 1999; Ingber and Jamieson, 1985).

Traditional tools in molecular cell biology cannot be used to test these biophysical hypotheses. Instead, we have had to miniaturize different types of engineering

analysis methods, to develop new ones, and to combine them with novel molecular cell biological approaches to test the tensegrity theory and gain greater insight into cellular biophysics. Initially, we devised methods to control how cells physically interact with ECM substrates in order to test directly whether cell shape distortion influences intracellular biochemistry and cell behavior. Results of these studies confirmed that mechanical forces functioned as bioregulators.

We then shifted our focus to explore how cells sense and respond to mechanical forces at the molecular level. Due to the small size of living cells and our desire to determine the contributions of discrete cytoskeletal filament networks, integrins, ECM, and cytoskeletal prestress to cell mechanics and mechanotransduction, these methods needed to provide the ability to apply controlled forces to specific molecules while simultaneously measuring changes in molecular displacement and biochemical activities inside the cell at the nanometer scale. Additional insight into cell structure and mechanotransduction came from the development of different methods that provided ways to physically disrupt discrete cytoskeletal elements with nanometer resolution in living cells, without interfering with the function of other cellular components or compromising cell viability.

By applying these methods to systematically analyze the molecular basis of cellular mechanotransduction, and combining these techniques with methods developed by other laboratories, such as traction force microscopy, we confirmed that mechanochemical conversion is mediated by forces channeling through integrins and the cytoskeleton. Our results also provide direct experimental evidence that cells use tensegrity to mechanically stabilize themselves (Brangwynne *et al.*, 2006; Kumar *et al.*, 2006; Lele *et al.*, 2006; Maniotis *et al.*, 1997; Wang *et al.*, 1993). In addition to providing new analytical approaches to study cellular biophysics and mechanotransduction, some of these methods are beginning to be adapted to provide novel biomaterial control interfaces, and they may facilitate integration of living cells into machines (e.g., biochips, medical devices, biodetectors, computers) in the future.

II. Control of Cell Shape, Cytoskeletal Organization, and Cell Fate Switching

On the basis of past work from cell and developmental biology, and the concept that cells and tissues might use tensegrity architecture, we proposed over 20 years ago that the spatial differentials of cell growth and function that drive tissue morphogenesis might be controlled mechanically through local variations in physical interactions between cells and their ECM (Huang and Ingber, 1999; Ingber and Jamieson, 1985). Changes in the cellular force balance would produce both local and global cytoskeletal rearrangements inside the cell and thereby, drive changes in intracellular biochemistry that influence cell fate decisions such as whether cells will grow, differentiate, or die. In early studies, we developed a

method to control cell shape by varying the density of ECM molecules coated on otherwise nonadhesive dishes; cells spread on surfaces with high ECM-coating densities, but retracted and rounded on low coating concentrations (Ingber and Folkman, 1989b). In addition, adherent cells, such as capillary endothelial cells (Ingber, 1990; Ingber and Folkman, 1989a) and primary hepatocytes (Mooney *et al.*, 1992), respond to growth factors and proliferate when spread, whereas they differentiate in the same medium under conditions that prevent cell extension (e.g., when adherent to low ECM densities). However, these results were difficult to interpret because, in addition to differences in cell shape, altering ECM-coating densities also may change the degree of integrin receptor clustering on the cell surface, which regulates the ability of these ECM receptors to activate intracellular signal transduction (Schwartz *et al.*, 1991).

We therefore set out to design an experimental system in which cell shape distortion could be varied independently of either the concentration of soluble hormones or the local ECM ligand-binding density. The approach we took was to microfabricate ECM islands of defined size, shape, and position on the micrometer scale, surrounded by nonadhesive barrier regions. Living cells exert traction forces on their ECM adhesions, and thereby spread and flatten themselves against standard culture substrates. Our approach was therefore based on the concept that cells would adhere to small ECM islands and extend themselves until they reached the nonadhesive barrier region where they would stop, and effectively take on the bounding shape of their "container." The degree of extension and flattening of single cells could therefore be controlled by plating the cells on different sized islands coated with the same high density of ECM molecule, in the same growth factor-containing medium; only the degree of cell distortion would vary. We accomplished this by adapting a microcontact printing technique that was initially developed as an alternative way to manufacture microchips for the computer industry by the laboratory of our collaborator, George Whitesides (Department of Chemistry and Chemical Biology, Harvard University) (Singhvi *et al.*, 1994; Whitesides *et al.*, 2001; Xia and Whitesides, 1998).

A. Microcontact Printing of Micropatterned Substrates for Cell Culture

The microcontact printing technique is a form of "soft lithography" which uses the elastomeric material, poly(dimethylsiloxane) (PDMS), to create flexible molds that retain the surface topography of silicon masters. The surfaces of silicon masters are, in turn, patterned using standard photolithography techniques which involves coating with photoresist polymer layers, exposure to UV light, removal of noncrosslinked polymers, and surface etching (Xia and Whitesides, 1998). These stamps can be used to transfer pattern elements and create multiple replica substrates when combined with chemical inks that form self-assembled monolayers (SAMs) (Prime and Whitesides, 1991).

We adapted this method to create patterns of ECM molecules that support cell adhesion in order to microengineer culture substrates with defined shapes and sizes

on the micrometer scale (Fig. 1). Typically for micropatterned substrates for cell-sized adhesive islands, the desired pattern is drawn using a computer-aided design software (e.g., AutoCAD), and printed on a transparent plastic sheet that functions as the photomask. The printing is done typically by commercial services with high-resolution laser printers, although masks with features in the order of hundreds of micrometers may be generated using a consumer laser printer. Standard photolithographic techniques are used to etch this pattern into a photoresist polymer layer (e.g., 2-μm thick coating of polymethylmethacrylate) that is coated over a planar silicon wafer to generate a "master" with topographic surface features corresponding to that of the photomask (Chen *et al.*, 1998; Chapter 13 by Sniadecki and Chen, this volume for more details). Liquid PDMS prepolymer (1:10 elastomer base:curing agent; Sylgard 184, Dow Corning) is poured over the master, cured at 60 °C for 2 h and then peeled away by hand. This procedure yields clear and flexible PDMS stamps with raised surface features that correspond precisely to the original photomask pattern (Fig. 1). To engineer cell culture substrates on the micrometer scale for experimental studies, the surface of the flexible stamp is inked with a cotton applicator stick saturated with an ethanolic solution of methyl-terminated long-chain alkanethiols (e.g., hexadecanethiol, Sigma, Missouri), dried with compressed nitrogen or argon, and brought into conformal contact for 30 sec with a clean gold substrate. The substrate is previously prepared by depositing a 40-nm layer of gold on a titanium-primed glass slide using an e-beam metal evaporator (note that this step involves the same equipment that is used for preparing samples for electron microscopy; Whitesides *et al.*, 2001). The PDMS stamp is applied to the gold-coated slide by placing the stamp onto the slide, and then pressed down lightly with a forceps or finger (Fig. 1) until the pattern is visibly in contact with the entire surface. This can sometimes be seen by a

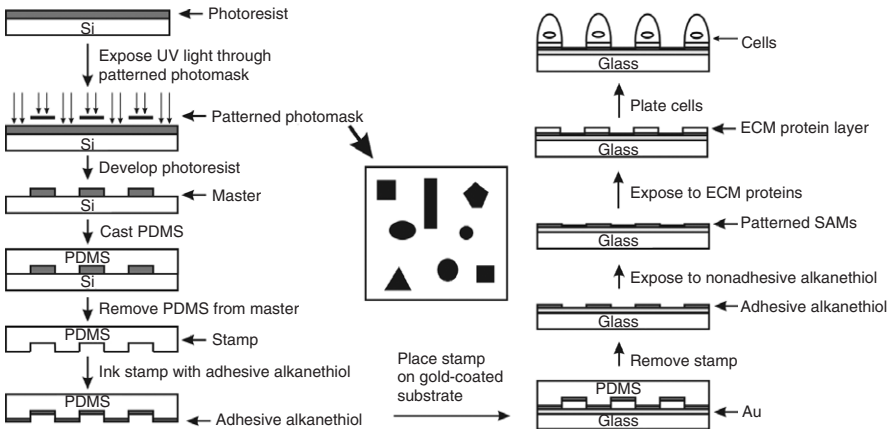

Fig. 1 Microcontact printing using soft lithography and SAMs. Method for microfabrication of stamps and microcontact printing SAMs on gold-coated glass substrates.

refraction of light on the substrate. Only the raised features of the stamp touch the gold and transfer the methyl-terminated alkanethiols within those geometrically defined regions to the surface of the substrate, where they self-assemble into a semicrystalline planar lattice (Xia and Whitesides, 1998). The PDMS stamps can be cleaned by sonicating in ethanol for 30 min and used repeatedly for several hundred times. The silicon master itself can be used to make hundreds of PDMS stamps if kept in a dust-free environment.

After removing the stamp, the glass substrate is covered with a solution of alkanethiol that is terminated with oligo(ethylene glycol) [OEG, e.g., $(EG)_3OH$]; this backfills all remaining (unstamped) areas of the exposed gold and thereby creates one single-planar SAM that covers the entire surface of the substrate, but exposes different terminal groups in different patterned regions. The substrate is then rinsed sequentially with ethanol, water, phosphate-buffered saline (PBS) and finally incubated in PBS containing ECM proteins (e.g., fibronectin, laminin, different collagen types) at a concentration of 50 μg/ml for 3 h at room temperature. After washing off excess protein (taking care not to allow the substrate to dry out) and transferring the substrates to culture medium, the microcontact-printed substrate is ready for cell culture.

As the terminal OEG groups of the alkanethiols within the barrier regions prevent protein adsorption, the soluble ECM proteins do not adhere to these regions. Instead, proteins preferentially adsorb to the patterned regions of the substrate that were stamped with methyl-terminated alkanethiols. Thus, this procedure results in creation of a microarray of adhesive ECM islands with the precise size, shape, and distribution depicted in the original photomask, surrounded by nonadhesive, OEG-coated barrier regions (Fig. 2A).

B. Application Notes on Microcontact Printing

For applications that require single cells to be confined within single adhesive islands, cell spreading and shape can be controlled with micrometer resolution by the size and shape of the islands, as long as the area of the island is equal to or less than the maximum area of spreading for that particular cell type (e.g., ~3000 and 4000 μm^2 for bovine and human endothelial cells, respectively; Chen *et al.*, 1998), and the nonadhesive spacing between adjacent islands is large enough to prevent cell spreading across multiple islands. For example, the spacing thresholds at which bovine and human endothelial cells can bridge across neighboring islands are 10 and 20 μm, respectively, and this bridging ability appears to be directly related to cell size (i.e., human endothelial cells are about twice as large as bovine) (Chen *et al.*, 1998). On the other hand, the interisland spacing cannot be made too large because this can lead to "sagging" of the PDMS stamp between neighboring islands and a loss of pattern fidelity. In short, both design features (i.e., island size and interisland distances) need to be determined empirically for each new cell type that is introduced into this experimental system. These studies can be carried out in

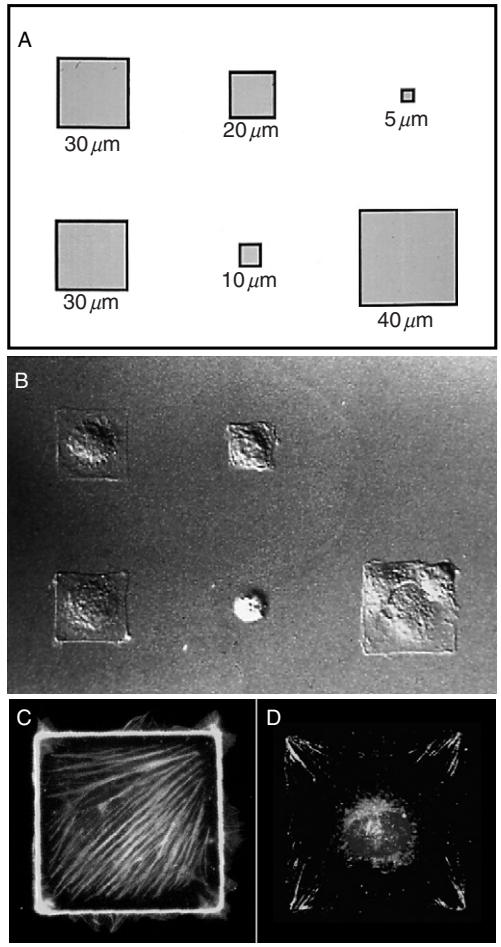

Fig. 2 Control of cell shape and cytoskeletal organization on micropatterned adhesive islands. (A) Schematic design of an array of different shaped square adhesive islands (top) and Nomarski microscopic images of bovine capillary endothelial cells plated on fibronectin-coated adhesive islands patterned according to this design using the microcontact printing method. Note that cells change their size and shape to match that of their adhesive islands. (Scale bar is 30 μm.) [Modified from Chen *et al.* (1997) with permission]. (C) Higher magnification fluorescence microscopic view of a cell cultured on a 40×40 μm^2 square ECM island and stained for actin fibers using Alexa488-phalloidin. Note that stress fibers orient preferentially along the diagonals (central nuclei are stained with DAPI). (D) A similar magnification view of another cell cultured on a similar island and immunostained for vinculin. Vinculin-containing focal adhesions concentrate within the corner regions at the points where the ends of stress fibers insert on the underlying ECM substrate. [Modified from Parker *et al.* (2002) with permission.]

medium with or without serum; however, the best shape control is generally observed under serum-free conditions.

The microcontact printing technique is extremely useful for holding single cells in particular configurations, as various types of adherent cells spread to take on the size and geometric form (e.g., square, triangle, circle, and so on) of the micro-engineered islands (Fig. 2A and B). Thus, it can be used to analyze directly the relation between cell shape and biological control. This method allowed us, for example, to demonstrate unequivocally that cell spreading produced through physical interactions between cells and their ECM adhesions can control cell fate decisions. Capillary endothelial cells, hepatocytes, and other cell types proliferated when allowed to spread on large (2500 μm^2) islands in the presence of soluble growth factors (Fig. 3A); however, they shut off growth and differentiated (liver cells produced blood proteins, capillary cells formed hollow tubes) when cultured on smaller islands that promote moderate spreading ($\sim$1000–2000 μm^2) in the same medium (Chen *et al.*, 1997; Dike *et al.*, 1999; Singhvi *et al.*, 1994). Moreover, capillary cells switched on the cellular suicide (apoptosis) program when grown on single tiny ($<$500 μm^2) ECM islands that induced almost complete cell rounding (Chen *et al.*, 1997; Fig. 3A).

As described above, when the interisland spacing is decreased, cells can bridge across multiple islands. We took advantage of this observation to culture capillary cells on multiple islands that had the size of individual focal adhesions (5 μm in diameter) and were closely spaced (10-μm apart). Under these conditions, each cell spread extensively (Fig. 3A), even though it contacted the same total amount of ECM area as when it was confined to single small ECM islands (10-μm diameter circles) that promoted apoptosis. In contrast to cells that were constrained in a round form on single 10-μm islands, cells that spread over many 5-μm islands proliferated, hence demonstrating that cell shape distortion is critical in governing cell life and death (Chen *et al.*, 1997).

Substrates created with microcontact printing are also extremely useful for analysis of the effects of physical interactions between cells and their ECM adhesions on intracellular cytoskeletal organization and focal adhesion formation. For example, immunofluorescence staining for vinculin within cells spread over a dense microarray of multiple small (3- to 5-μm diameter) ECM islands revealed that focal adhesion assembly is governed by the degree to which the entire cell can spread: cells held in a round form by attachment to single 10-μm ECM islands could not form well-developed focal adhesions (Chen *et al.*, 2003), even though they adhered to the same high ECM density. Moreover, the organization of the focal adhesion itself varied depending on the size of the island and its position beneath the cell, as well as on the level of tension in the cytoskeleton.

Analysis of cells cultured on larger (single-cell sized) square ECM islands revealed that intracellular stress fibers align predominantly along the diagonals of the square (Fig. 2C), while focal adhesions preferentially form at corners (Brock *et al.*, 2003; Parker *et al.*, 2002; Fig. 2D). Importantly, when the square cells were stimulated with motility factors, they preferentially extended lamellipodia,

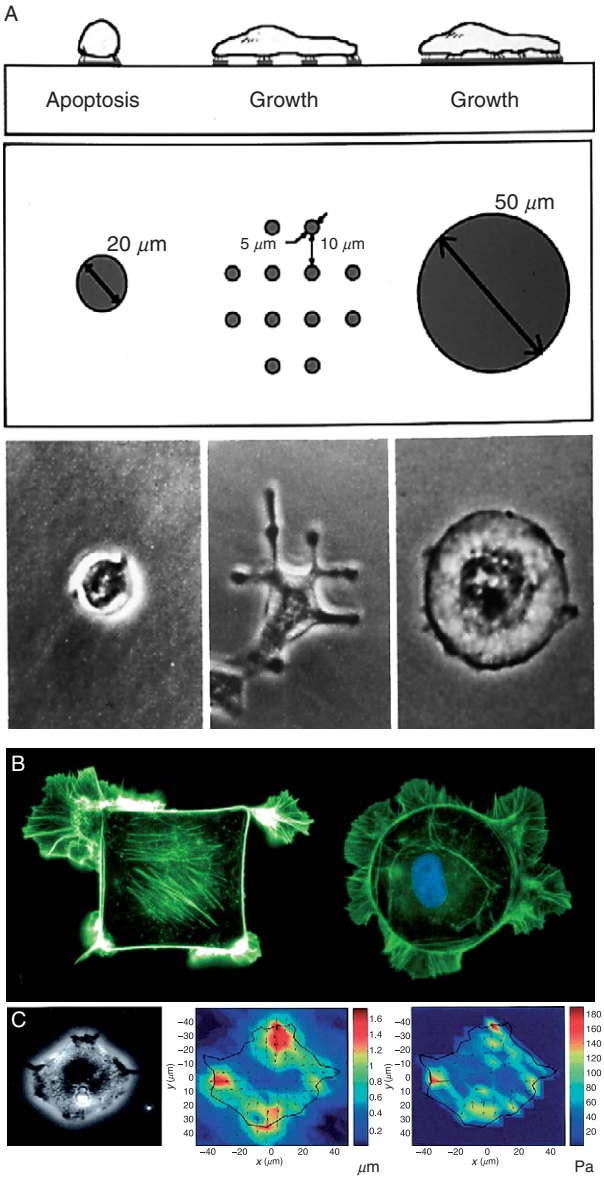

Fig. 3 Cell distortion-dependent control of cell function. (A) Top image is a schematic of a design for a micropatterned substrate containing single sparse small or large circular ECM islands, or a dense array of tiny (5 μm) focal adhesion-sized islands. The bottom phase-contrast microscopic images show that capillary endothelial cells take on the shape of the single small (left panel) or large (right panel) islands, but spread over multiple closely spaced tiny islands (middle panel). Spread cells proliferate whereas those that remain spherical undergo apoptosis even though the total amount of cell–ECM contact area is similar in cells on the single small island and multiple tiny islands. [Modified from Chen *et al.* (1997) with permission.] (B) Fluorescence staining of the actin cytoskeleton reveals that cells

filopodia, and microspikes from their corners, whereas there was no bias in round cells on circular islands (Parker *et al.*, 2002; Fig. 3B). Use of polygonal ECM islands with different shapes and numbers of corners, but similar size (900 μm^2), revealed that cells extend new motile processes more frequently from corners with acute, rather than obtuse angles (Brock *et al.*, 2003). By using the microcontact printing technique to microfabricate square ECM islands on the surface of flexible polyacrylamide gels used for traction force microscopy (Pelham and Wang, 1997; Wang and Pelham, 1998; Chapter 2 by Kandow *et al.*, this volume), we were able to demonstrate that cells exert greatest traction forces in these same corner regions (Wang *et al.*, 2002a; Fig. 3C). Separate studies revealed that lamellipodia extension can be inhibited by dissipating cytoskeletal tension (Brock *et al.*, 2003; Parker *et al.*, 2002). Thus, use of the microcontact printing method allowed us to demonstrate that global control of cell shape can result in spatial patterning of cytoskeletal prestress which, in turn, influences local molecular biochemical responses inside the cell, including the positioning of focal adhesions and lamellipodia that are central to directional cell motility. The microcontact printing technique also has been adapted for analysis of signal transduction and other biochemical studies (Chen *et al.*, 1998; Polte *et al.*, 2004). However, because cells must be plated sparsely to maintain single cells on individual islands, it is sometimes difficult to obtain large amounts of protein or RNA for biochemical analysis (i.e., many similar dishes must be cultured in parallel).

C. Extension and Future Development of Microcontact Printing

Taken together, these studies show that microfabricated ECM islands allow one to discriminate clearly between signals conveyed by soluble factors, direct binding of immobilized ECM molecules, and physical cues associated with cell shape distortion. For this reason, this method or modified versions of this technique (Tan *et al.*, 2004) are now a mainstay in studies on the mechanisms by which cell shape and behavior are controlled by physical interactions between cells and ECM. The microcontact printing method could also be modified by directly conjugating peptides that mediate integrin receptor binding and cell adhesion (e.g., RGD cell-binding site from fibronectin) to the terminal (EG)OH group of the OEG-alkanethiol (Kato and Mrksich, 2004; Roberts *et al.*, 1998). Use of these SAMs eliminates the need to add ECM protein to the substrate, as they are themselves sufficient to promote cell attachment, spreading, and growth (Roberts *et al.*, 1998).

---

stimulated with motility factors (e.g., FGF, PDGF) preferentially extend new motile processes (e.g., lamellipodia, filopodia) from their corner regions when cultured on square ECM islands (left), whereas cells on circular islands do not display this preference (right). (C) Phase-contrast (left) and traction force microscopic images of substrate displacements (middle) and traction fields (right) beneath cells cultured on square ECM islands that are fabricated on the surface of flexible polyacrylamide gels. Traction forces concentrate in the corner regions where new lamellipodia preferentially form. [Modified from Parker *et al.* (2002) with permission.]

New ECM proteins secreted by cells cannot adsorb to these RGD-coated substrates because of the dense, underlying layer of (EG)OH groups, thus these substrates may be particularly useful for studies that are designed to discriminate between direct "outside-in" signaling from the ECM substrate versus signaling mediated by *de novo* deposition of new proteins by the adherent cells.

Microcontact printing is convenient and suitable for patterning large areas of a surface (up to $\sim$100 cm^2) with multiple adhesive islands in a single printing. It can routinely transfer patterns with island features having dimensions on the size of 1 μm with an edge roughness of $\leq$100 nm (Xia and Whitesides, 1998). This resolution is more than sufficient for control of cell shape and position; however, it can be enhanced with some additional steps to create patterns with 40-nm features if nanoscale control is desired (Rogers *et al.*, 1998). Multiple methodological improvements also have been made. For example, one modification allows direct printing of proteins onto PDMS-coated substrates, thereby removing the need for special metal-coating equipment (Tan *et al.*, 2004; Chapter 13 by Sniadecki and Chen, this volume). This method overcomes some major limitations of the original microcontact printing technique, namely the unsuitability of gold substrates for microfluorimetry (e.g., calcium imaging) and the high cost of materials. Direct stamping of PDMS also allows visualization of live cells at high magnification, by printing proteins onto PDMS-coated coverslip-bottomed dishes (MatTek).

Finally, multiple electrochemical (Jiang *et al.*, 2005; Yeo *et al.*, 2001, 2003; Yousaf *et al.*, 2001) and optochemical (Ryan *et al.*, 2004) methods also have been incorporated into the microcontact printing technique. These modifications allow dynamic and localized alteration of the chemical composition of micropatterned substrates, and enable reversible or dynamic control over cell behaviors. For example, some of these substrates permit rapid release of an adherent cell from the physical constraints of its island, by converting surrounding nonadhesive barrier areas into adhesive regions, and thus may be particularly useful for studies on directional cell motility. The power of this method lies in the creativity of the investigator.

III. Probing Cell Mechanics, Cytoskeletal Structure, and Mechanotransduction

A number of models predict that mechanical stresses are not transmitted equally across all points on the cell surface. For example, the cellular tensegrity model was one of the first to suggest that forces will be preferentially transferred across transmembrane adhesion receptors, such as integrins, that physically anchor the cytoskeleton to the ECM (Ingber, 1991; Ingber and Jamieson, 1985). Moreover, if the cytoskeleton behaves like other tensegrity structures, then its mechanical stiffness should vary as a function of cytoskeletal prestress. To test these hypotheses, we needed to develop a method to apply controlled mechanical stresses to integrins and other surface proteins on living cells, and simultaneously measure

changes in cell and cytoskeletal mechanics. We first accomplished this by developing a magnetic twisting cytometry (MTC) technique in which controlled shear forces are applied to surface receptors via bound ligand-coated ferromagnetic microbeads (Wang *et al.*, 1993). We later developed related magnetic pulling cytometry (MPC) methods that apply tensional forces to superparamagnetic beads coated and bound in a similar manner (Alenghat *et al.*, 2000; Matthews *et al.*, 2004b; Overby *et al.*, 2005).

Magnetic techniques offer a number of advantages over other methods that are commonly used to probe cell mechanics such as optical tweezers (Dai and Sheetz, 1995) and atomic force microscopy (Shroff *et al.*, 1995). While all these methods can apply localized forces to molecules on the cell surface, the advantages of micromagnetic techniques include: (1) a much wider range of stress (from piconewtons to many nanonewtons) can be applied to specific cell surface receptors, (2) a much larger frequency range (0–1000 Hz) of forces can be applied, (3) hundreds to thousands of cells and bound beads can be analyzed simultaneously, (4) cells may be mechanically probed continuously for hours or even days without potential heating problems, (5) forces can be applied inside cells by allowing cells to engulf the beads, and (6) magnetic systems are more robust, easier to use, and cheaper to build.

A. Magnetic Twisting Cytometry (MTC)

MTC uses ferromagnetic microbeads (1- to 10-μm diameter) to apply twisting forces (shear stresses) to specific receptors on the surface membrane of living cells. Carboxylated ferromagnetic beads (4.4-μm diameter; Spherotek) are coated with ligand (e.g., ECM molecules, RGD peptide from the cell-binding region of fibronectin, receptor-specific antibodies) by incubating the beads (5 mg) with 1 mg/ml of ligand in 0.1-M sodium phosphate buffer (pH 5.5) containing 1-mg/ml 1-ethyl-3 (-3-dimethylaminopropyl)carbodiimide (EDAC) for 2 h with gentle agitation to prevent settling. Coated beads are rinsed twice and stored in sterile PBS containing 0.1% BSA for up to 1 week at 4 °C. For experiments, coated ferromagnetic beads are added to the cells (~20 beads/cell) in serum-free, chemically defined medium and incubated for 10 min at 37 °C followed by gentle washing three times with PBS to remove unbound beads prior to force application. To apply twisting forces to beads and bound surface receptors, a strong (1000 G) but very brief (10 μsec) magnetic pulse is applied to the receptor bound ferromagnetic beads using a horizontal Helmholtz coil (Fig. 4A). This induces and aligns the magnetic dipoles of the beads in the horizontal direction. Within a few seconds, a weaker (0–80 G), but sustained, magnetic field is applied in the perpendicular direction using a second vertically oriented Helmholtz coil. As a result, the beads are twisted, thus applying shear forces directly to the bound receptors. The average bead rotation and angular strain induced by the twisting field is measured using an in-line magnetometer (Valberg and Butler, 1987; Fig. 4B), and rotational shear stress is computed (see next paragraph) based on knowledge of the twisting field and angular strain of the bead (mechanical anisotropy of the cell may affect the degree

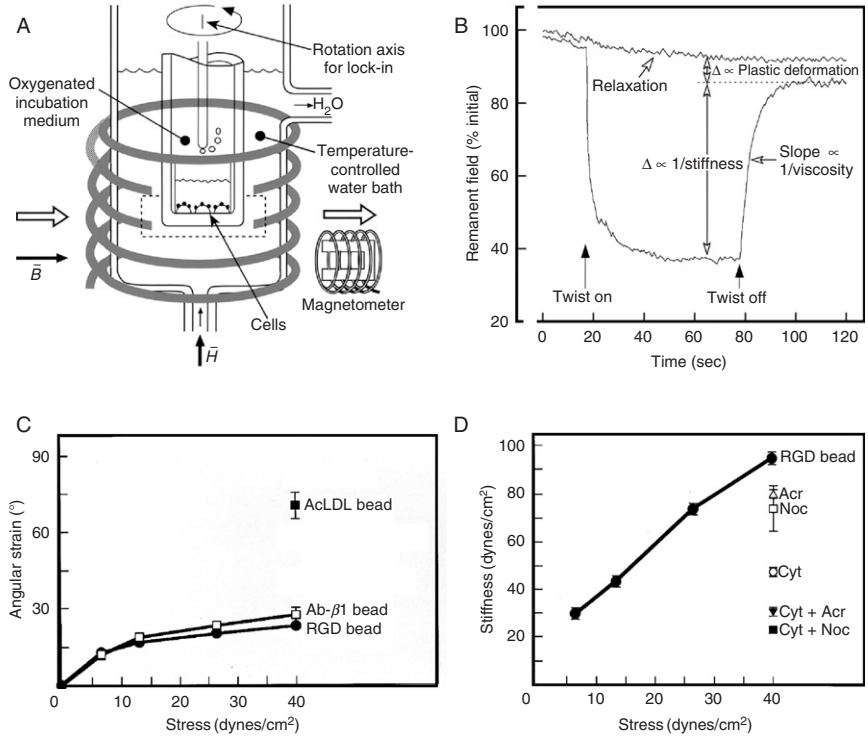

Fig. 4 Magnetic twisting cytometry. (A) Schematic diagram of the magnetic twisting cytometer [modified from Wang *et al.* (1993) with permission]. Small tubes (single wells of detachable 96-well plates) containing cells and bound ferromagnetic beads are placed in medium in a central tube and gassed with 95% O_2/5% CO_2 in the temperature-controlled water-jacketed chamber. A 1000-G horizontal magnetic field (B) is used to magnetize the beads with a pair of horizontal magnetic coils (open arrows). The magnetic field generated by the magnetized beads (horizontal closed arrow) is measured by an in-line magnetometer. Next, a perpendicular 30-G magnetic field (H) applied by a vertical coil outside the chamber (vertical closed arrow) is used to twist the beads. Ambient magnetic noise is minimized by appropriate orientation of the four magnetometer probes, an external superalloy shield, and rotating the entire chamber around the vertical axis at 10 Hz. (B) An example of data obtained from MTC analysis of normal cardiocytes. The relaxation curve (relaxation) represents spontaneous remanent field decay in the absence of a twisting field. Cytoskeletal stiffness is inversely related to the extent of the decrease in the remanent field after the twisting field is applied, and cytoskeletal apparent viscosity is inversely related to the slope of remanent field recovery after the twisting field is removed. The residual angular strain representing permanent cytoskeletal deformation after twisting field removal is also indicated (plastic deformation). (C) Stress–strain relation in living capillary endothelial cells measured with bound ferromagnetic beads coated with ligands for transmembrane integrin receptors (anti-β1 integrin antibodies, synthetic RGD peptide) or control transmembrane metabolic acetylated low-density lipoprotein (AcLDL) receptors [modified from Tagawa *et al.* (1997) with permission]. Cells preferentially stiffen and exhibit decreased bead rotation (as evident from the flattening of the rotational stress–angular strain curve), when twisting forces are applied to integrins. Angular strain was calculated as the arc cosine of the ratio of remanent field after 1 min of twist to the field at time 0. Applied stress was determined as described in the text. (D) Cell stiffness (ratio of stress to strain in radians after 1-min twist) measured through integrin bound ferromagnetic beads in the absence or presence of cytochalasin

of angular rotation of the bead). In this manner, the mechanical behavior of the integrins linked to the cytoskeleton can be characterized in living cells by measuring stress–strain responses (Fig. 4C and D), as well as analyzing creep and elastic recoil behavior (Wang and Ingber, 1995; Fig. 4B). Here we describe how several biomechanical parameters (stiffness, permanent deformation, and apparent viscosity) are measured.

The applied torque T_{mag} is given by $T_{mag} = \mu_0 \mathbf{M} \times \mathbf{H}_a$, where μ_0 is permeability of free space, vector $\mathbf{M}$ is the microbead magnetic moment, and $\mathbf{H_a}$ is the external twisting field. Since the specific gravity of magnetic beads is much lower than 10^4 (Wang and Ingber, 1994), we can neglect inertial effects; thus the net torque on the microbead is assumed to be zero. If we assume that elastic and viscous contributions are mechanically in parallel, then their torques are additive. Therefore, $T_{mag} = T_{elas} + T_{vis}$ where T_{elas} and T_{vis} are elastic and viscous (or frictional) torques, respectively (assuming that cells generate negligible torques to resist the applied magnetic torque). This gives $\mu_0 \mathbf{M} \mathbf{H}_a \sin\theta = -\kappa V \eta \omega + \kappa V E(90° - \theta)$ where θ is the angle between $\mathbf{M}$ and $\mathbf{H}_a$, κ is the particle shape factor and equals 6 for a spherical microbead, V is the microbead volume, η is the viscosity, and ω is the angular velocity of the microbead rotation and equals $d\theta/dt$.

The value θ above is also the angular strain of the microbead induced by the twisting field. To correct for the effects of relaxation (i.e., force-induced cell remodeling), we assume that twisting-induced rotation and relaxation are two independent processes so that $\theta = 90° - \cos^{-1}[B(t)_{twist}/B(t)_{relax}]$. $B(t)_{twist}$ is the magnitude of the remanent field (i.e., the magnetic induction that remains in the material after removal of the applied twisting field that is measured by the in-line magnetometer in the magnetizing direction). $B(t)_{relax}$ is the remanent field resulting from the relaxation by the cell and is measured by the in-line magnetometer at the steady state after the twisting field is turned off. The applied stress $\sigma = cH_a[B(t)_{twist}/B(t)_{relax}]$, where H_a is the applied external field and c is the bead calibration constant that is determined by placing the bead in a viscous standard (Wang and Ingber, 1994). Thus, the applied shear stress σ and angular strain θ can be calculated, from which the cell stiffness E can be computed as $E = \sigma/\theta$, the ratio of stress to angular strain. Permanent deformation is defined as the nonrecovered bead rotation after the twisting field is turned off (i.e., when applied stress is removed; Fig. 4B) relative to the bead rotation when the stress is applied, and is given by $(\theta_2/\theta_1) \times 100\%$ where 2 and 1 represent states when the applied stress is on and off, respectively).

D (CytoD) which disrupts the actin cytoskeleton in living cells. Cellular stiffness increases linearly with stress. The stiffness dramatically decreases when cells are treated with CytoD, nocodazole (Noc), or acrylamide (Acr) to disrupt microfilament, microtubule, or intermediate filament integrity, respectively [modified from Wang *et al.* (1993) with permission]. Each agent alone only produced partial inhibition, whereas combination of multiple agents completely inhibited the cell-stiffening response. These results show that the mechanical resistance measured through integrins is due to an integrated cytoskeletal strengthening response that involves all three filament systems.

Cellular viscosity is obtained by measuring the time course of the disappearance of angular strain θ when the applied field is turned off. The equation above gives $\kappa V\eta\omega = \kappa VE(90^\circ - \theta)$, solving this differential equation yields $\phi = \phi_0 e^{-t/(\eta/\epsilon)} = \phi_0 e^{-t/(\tau)}$ where $\phi = 90^\circ - \theta$, $\phi = \phi_0$ at $t = 0$ and $\tau = \eta/E$; the later relation allows the estimation of cell viscosity through knowledge of τ and E. τ is defined as the time when $\phi = \phi_0(e^{-1}) = 0.34\phi_0$ and is measured experimentally. Thus, MTC can be used to obtain cell stiffness, cell apparent viscosity (frictional contribution), and permanent deformation (remodeling associated changes) of the cell and cytoskeleton when controlled shear stresses are applied to different cell surface receptors.

B. Applications of MTC

The MTC technique was used to demonstrate directly that forces applied to integrins and nonadhesion receptors on the same cell produce different responses. For example, beads bound to integrins via RGD ligands or anti-β1 integrin antibodies exhibited significantly less angular rotation in response to applied magnetic field, compared to beads bound to transmembrane receptors that do not physically couple to the internal cytoskeleton such as metabolic receptors, growth factor receptors, or histocompatibility antigens (Wang *et al.*, 1993; Yoshida *et al.*, 1996; Fig. 4C). The mechanical stiffness of many different types of cells also was found to increase in direct proportion to the level of applied shear stress (linear strain-hardening behavior) (Fig. 4D). Use of specific pharmacological modifiers or genetic knockout techniques further revealed that all three cytoskeletal filament systems—actin microfilaments, microtubules, and intermediate filaments—contribute to this mechanical response (Fig. 4D). Moreover, cell stiffness varied with cytoskeletal prestress: increasing basal levels of tension in the cytoskeleton using stimulators of actomyosin interactions made the cells more rigid, whereas dissipating tension immediately increased cell flexibility (Wang *et al.*, 2002b). A mathematical formulation of the tensegrity model predicts this behavior (Coughlin and Stamenovic, 1998, 2003; Laurent *et al.*, 2002; Stamenovic *et al.*, 1996).

The MTC method also has been used to determine how different transmembrane adhesion receptors, including various types of integrins, cadherins, selectins, and urokinase receptors (Potard *et al.*, 1997; Wang and Ingber, 1995; Yoshida *et al.*, 1996), differ in their ability to support transmembrane mechanical coupling to the cytoskeleton. Additionally, when the same stress was applied to different-sized magnetic beads (e.g., 4.5-μm vs 1.4-μm diameter), larger beads appeared to be stiffer or more resistant to rotation than smaller beads (Wang and Ingber, 1994). This result is consistent with the idea that, when applied to beads ligated to integrins, MTC probes the underlying 3D structure of the cytoskeleton rather than the 2D structure of the cell's surface membrane (Stamenovic and Coughlin, 2000).

C. Extension and Future Development of MTC

MTC has been combined with signal transduction experiments to analyze the molecular basis of cellular mechanotransduction. For example, MTC was used to show that shear stress applied to integrin receptors activates the cAMP signaling pathway and leads to mechanical activation of gene transcription driven by cAMP response elements (Meyer *et al.*, 2000). Importantly, application of the same stress to beads bound to transmembrane metabolic receptors or to nonactivated integrin receptors (i.e., that do not have the RGD-binding site occupied) did not activate cAMP signaling in these cells, demonstrating that mechanical deformation of the plasma membrane alone is not sufficient to activate this mechanotransduction pathway.

MTC also has been combined with high resolution *in situ* hybridization to reveal that mRNA and ribosomes are simultaneously recruited to focal adhesions that form on the cytoplasmic face of surface-bound magnetic microbeads coated with integrin ligands, but not with ligands for other receptors (Chicurel *et al.*, 1998). When shear stress was applied to integrins through these beads using MTC, mRNA and ribosome recruitment was significantly augmented, and this response was suppressed by inhibiting cytoskeletal tension generation. These findings suggest that rapid posttranscriptional changes in gene expression may be mediated by repositioning of translational components to sites of signal reception and that the level of prestress in the cytoskeleton governs this response. In addition, force application via MTC was shown to regulate endothelin-1 gene expression in a prestress-dependent manner (Chen *et al.*, 2001).

Finally, MTC can be used both with large populations of cells to obtain averaged rheological properties and at the single-cell level with simultaneous microscopic visualization. The latter is achieved by fabricating a device containing orthogonal Helmholtz coils that can be placed on a microscope stage. When placed on a microscope, twisting forces are applied to many beads on a cell while using optical techniques to analyze local structural and biochemical responses of beads located in particular positions on the cell surface, or inside the cytoplasm (when engulfed, the degree of engulfment can be determined by cytoskeletal immunostaining after fixation or using GFP-tagged cytoskeletal proteins in live cells). Modified versions of the MTC method also have been developed to characterize dynamic cell mechanical behavior (oscillatory MTC; Fabry *et al.*, 2001), to apply forces in multiple directions (3D MTC; Hu *et al.*, 2004), and to explore force-induced displacements of molecular elements inside the cytoplasm and the nucleus (3D magnetic tomography; Hu *et al.*, 2003, 2004). Because these methods combine MTC with high-resolution microscopic imaging methods, nanoscale displacements of the bead can be measured in conjunction with measurements of changes in cytoskeletal elements in the cytoplasm and nucleus to explore how mechanical stresses are distributed throughout the cell (Chapter 8 by Wang *et al.*, this volume for more details).

D. Magnetic Pulling Cytometry (MPC)

MPC, also known as magnetic tweezers, is a related magnetic micromanipulation technology that can also apply forces to specific surface receptors through bound ligand-coated microbeads and measure local cell rheology. However, the technique differs from MTC in that superparamagnetic beads (4.5 μm; Dynal) are utilized instead of ferromagnetic beads, and a magnetic needle is used to apply tensional forces locally to individual surface receptor-bound beads on single cells (i.e., rather than global shear stresses to large populations of cells). Unlike ferromagnetic beads that maintain their magnetic moment, the induced magnetic moment disappears from superparamagnetic beads on the removal of external magnetic field. One advantage of this method over MTC is that large-scale distortion of the cell can be produced, whereas MTC only twists the beads in place. This method is especially well suited for studying force-induced changes of the mechanical properties and biochemical signaling functions at focal adhesions or other receptor-mediated anchoring complexes in single living cells.

Our group has fabricated magnetic needles that utilize either a stationary permanent magnet (Fig. 5) or an electromagnet to induce bead magnetization (Alenghat *et al.*, 2000; Matthews *et al.*, 2004a,b, 2006; Overby *et al.*, 2004, 2005; Figs. 6 and 7). The advantage of the permanent magnetic needle is that virtually any investigator can assemble one of these devices in a short time at minimal cost. Fabricating the electromagnetic needle is more involved and expensive, but it offers a wider range of dynamic control (Fig. 7) as well as higher levels of force application (up to 50 nN). Thus, a permanent magnetic needle is ideal for quick, preliminary experiments to test hypotheses, whereas the electromagnetic needle is preferred for studies involving more rigorous characterization.

The size and shape of the tips of the magnetic needles used in both devices are designed to maximize magnetic field gradient intensity while minimizing their size, so that they can be positioned as close to the cell membrane as possible (Fig. 6D). This is important because the magnetic field increases exponentially with decreasing distance to the needle tip (Fig. 5B and C). All magnetic needles can be calibrated by pulling the magnetic beads through a glycerol solution with a known viscosity (1 kg/m/sec or 1000 cP) (Fig. 5B). After recording the beads' velocities through the fluid, Stokes' formula for low Reynolds number flow, force $= 3\pi\eta Dv$, is used to deduce the forces on the beads, where η is the viscosity of the fluid, D is the bead diameter, and v is the velocity of the bead through the fluid. Due to the strong dependence of magnetic forces on distance, it is important that the magnetic needle be placed at the identical position during calibration as used during experimental manipulation.

The permanent magnetic microneedle system (Matthews *et al.*, 2004b) consists of a standard stainless steel needle attached to a permanent neodymium iron boron disk magnet (Edmund Industrial Optics, New Jersey) attached to an aluminum rod that is mounted on a microscope micromanipulator (Eppendorf, Germany) (Fig. 5A). To measure the local mechanical properties of bound receptors and

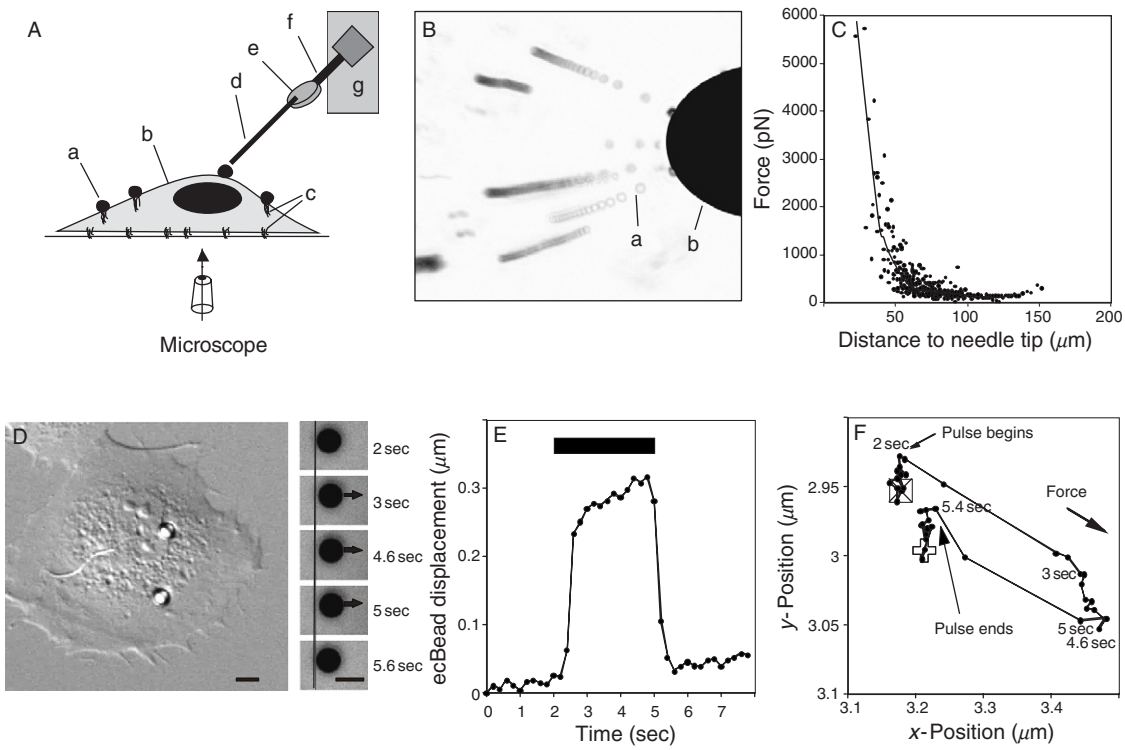

Fig. 5 Magnetic pulling cytometry. (A) Schematic of the permanent magnetic needle device. Ligand-coated superparamagnetic microbeads (a) bind and cluster receptors on the surface of cultured cells (b). When integrins are clustered, focal adhesions (c) form at the site of bead binding. A magnet microneedle consisting of a stainless steel needle (d) attached to a permanent magnet (e) fastened to an aluminum rod (f) that is mounted on a micromanipulator (g) is used to apply force to the receptor-bound beads, while viewing the cell and measuring bead displacements using an optical inverted microscope. (B) Forces applied to the beads are estimated by carrying out control studies as visualized in this composite of time-lapse images of bright-field views showing magnetic microbeads being pulled through glycerol in response to magnetic stress application by the microneedle. The beads (a) are attracted to the magnet along magnetic field lines perpendicular to the needle tip (b); forces exerted on individual beads are calculated using the Stokes equation as described in the text. (C) Force exerted on individual 4.5-μm diameter superparamagnetic Dynal beads as a function of the distance from the tip of the magnetic needle (calculated from data shown in B). (D) A Nomarski microscopic view of an adherent endothelial cell with two 4.5-μm RGD beads bound to integrins on its apical surface. A series of higher magnification bright-field images recorded over ~6 sec showing bead displacement to the right in response to application of a similarly oriented force (130 pN) pulse between 2 and 5 sec of the recording period (arrows) is shown at the right. (Scale bar is 5 μm.) (E) Bead displacement as a function of time before, during, and after the 3 sec force pulse (solid rectangle). (F) Map of changes in the positions of the bead measured in E during the same time course. Note the bead does not return to its original position after the force pulse ceases. [Modified from Matthews *et al.* (2004b) with permission.]

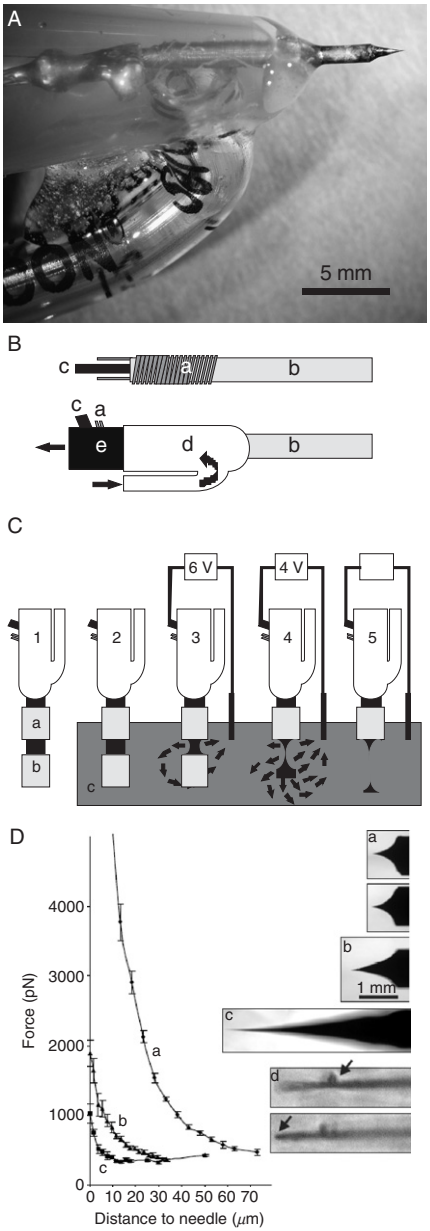

Fig. 6 The electromagnetic needle device for magnetic pulling cytometry. (A) Photograph of the pole tip of the electromagnetic needle device and integrated cooling system. (B) Diagram of the internal (top) and external (bottom) views of the magnetic needle system. A 50-μm diameter insulated copper electromagnet wire (a) is wound around a 1-mm diameter soft permalloy magnet core (b) and a 1.5-mm insulated copper wire (c) is soldered to the proximal end of the magnet core for electropolishing.

cytoskeletal linkages at bead-binding sites, cells with bound beads are maintained at 37 °C using a heated stage (Omega Engineering, Inc., Connecticut) and visualized on an inverted microscope (Nikon Diaphot 300, Japan). The magnetic needle is then used to apply force pulses to the bead, by moving the tip momentarily to the vicinity of the cell, while bead displacement is measured optically (Fig. 5D). To accomplish this, the manipulator speed is set to 1000 μm/sec, and the magnet tip is oriented at 45° relative to the substrate and positioned initially in the culture medium 600-μm away from the cell-bound beads to be tested. The needle tip is moved rapidly within 70–125 μm from the bead, held in position for any time desired (generally between 1 sec and 5 min), and then quickly returned to its original position using the micromanipulator. Time-lapse imaging (4 Hz) with a CCD camera (Hamamatsu, Japan) attached to the microscope is used to record bead motion. The centroid position of each bead is then determined frame by frame using IPLab (version 3.2.4, Scanalytics, Inc., Virginia), and the maximum bead displacement computed (Fig. 5E and F). To minimize cumulative effects from multiple force pulses, subsequent force pulses are applied to cells in the same dish that are >2-mm away from previously stimulated cells.

The electromagnetic needle device (Matthews *et al.*, 2004a) is powered by a simple voltage source and both the magnetic field and micromanipulator are controlled by a computer (Fig. 7). The electromagnetic needle is fabricated by winding multiple (>1000) loops of insulated electromagnet copper wire (25- to 50-μm diameter; Matthews *et al.*, 2004a) around a magnetic permalloy core in one or more layers (a 121-mm diameter composed of 81% nickel/19% iron can be obtained from Fine Metals Corporation, Ashland, Virginia; the permalloy core is annealed separately by Amuneal Manufacturing Corporation, Philadelphia, Pennsylvania) (Fig. 6B). The proximal portion of the permalloy core and the entire

The core with wound wire is placed within a thermoregulating water jacket (d) fashioned from a 1.5-ml Eppendorf tube with the exposed tip of the core extending through its distal surface. Arrows indicate direction of water flow through jacket and into a plastic outflow tube (e). (C) Electropolishing method for modification of pole tip geometry. (1) Two protective plastic cylindrical masks (a, b) are placed over the surface of the permalloy core tip so that the tip is completely covered and a controllable region of the core between the masks is exposed. (2) The tip with masks is then lowered into an acid solution (c). (3) An electric current (solid arrows) applied with a power supply set at 6-V DC is passed through the permalloy core thereby electrochemically polishing the exposed surface of the permalloy core. Once the core narrows by 50%, the distal plastic cap is removed and electropolishing is continued at 4 V (4) until the distal end of the permalloy core breaks off; the current is then shut down (5). The initial surface area of exposed core in step 1 determines final tip geometry. (D) Control of the magnetic field gradient by altering pole tip geometry. Needle pole tips with different tapered shapes of increasing lengths were created by exposing different areas of the core using different initial separations between the two plastic masks of 1.5 mm (a), 3 mm (b), 6 mm (c), and 15 mm (d) during the electropolishing procedure. In (d), 100× magnification images focused at the arrow indicates a 250-nm magnetic bead on shaft of needle tip (top), and 100-nm radius needle tip (below). Repeated fabrication protocol produced similar tip geometries (a). The lines indicate the force–distance relationship for respective pole tip geometries measured using 4.5-μm magnetic beads in glycerol as described in Fig. 5. [Modified from Matthews *et al.* (2004a) with permission.]

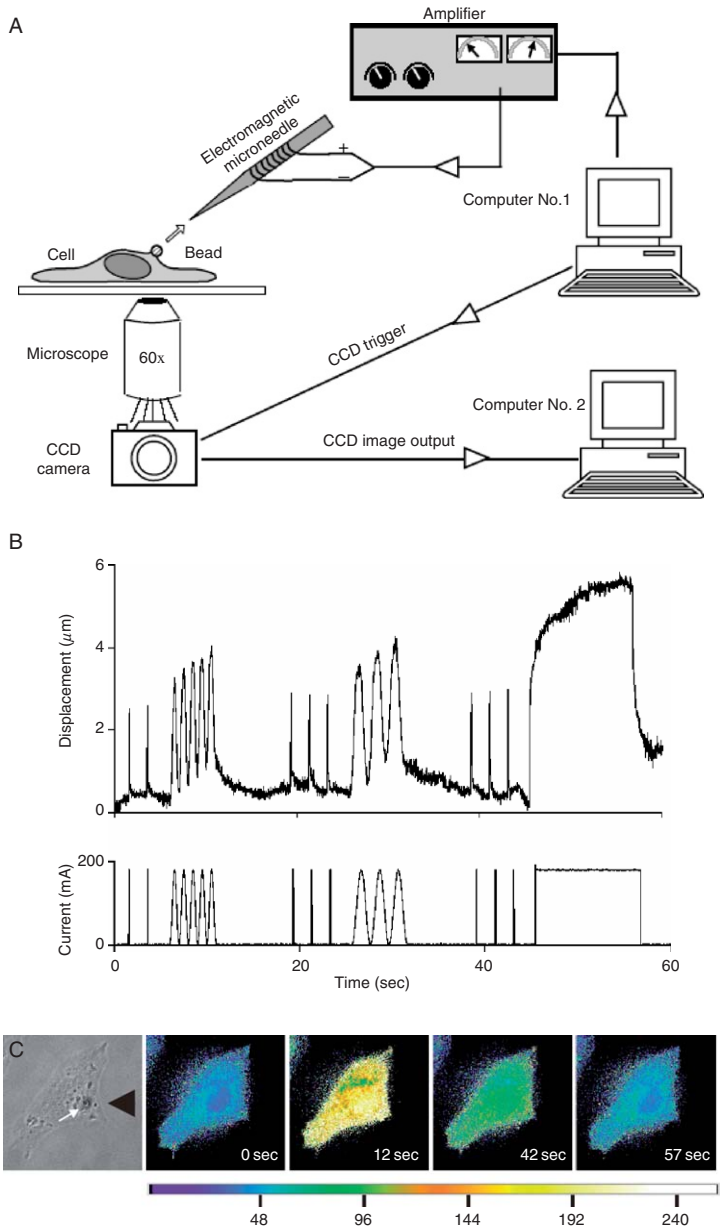

Fig. 7 Electromagnetic pulling cytometry for analysis of cell mechanics and mechanotransduction. (A) Experimental system. A ligand-coated superparamagnetic bead is bound to receptors on the surface of a living cell, while a magnetic force (arrow) is applied to the bead using the electromagnetic microneedle. An amplifier supplies current to the electromagnetic microneedle and is controlled using LabVIEW on computer No. 1 to generate any arbitrary user-defined force regimen. The bead

electromagnet coil are housed within a temperature-regulated water chamber (Fig. 6A).

The tip of the permalloy core of the electromagnet can be electrochemically sharpened (Fig. 6C) to between 200-nm and 20-μm diameter depending on the desired application, as magnetic field gradient intensity increases with tip curvature (Fig. 6D). To generate conical-shaped shafts with fine tips, two cylindrical plastic shields (1-mm internal diameter) cut from the ends of 200-μl Eppendorf pipette tips are fit over the ends of the core, leaving an exposed section of core between them (Fig. 6C). The pole tip is then immersed into a solution containing 8:7:5 phosphoric acid, sulfuric acid, and water, and a 6-V potential is applied through the permalloy and the acid solution to electropolish (etch) the exposed surface of the rod. When the diameter of the exposed material reaches ~40–50% of its original size, the potential is stopped, the distal plastic shield removed, and the electropolishing is resumed at 0–4 V (for better control) until the distal portion of the permalloy tip falls off. Progressively increasing the spacing between the shields results in a gradual increase in the taper. Continued electropolishing after the distal portion of the permalloy tip has fallen off results in a progressively duller tip and shorter neck.

One major problem associated with the use of small-scale electromagnets is the resistive heating of the electromagnet which can locally denature biomolecules and injure living cells, while also causing thermal expansion and movements of the electromagnet core. This movement, which can be 15–20 μm, eliminates precise control over the distance between the magnetic particle and the tip of the electromagnet, thereby hindering accurate control of the forces applied. We therefore incorporated a temperature-regulating water flow chamber (Fig. 6A) to ensure that the tip temperature remains within the design range of less than 2 °C variation and eliminates the possibility of the coil melting during application of currents beyond a brief pulse (>500 msec).

We use tosyl-activated superparamagnetic beads (4.5-μm diameter; Dynabeads M-450, Dynal) that are coated with receptor ligands by incubating the beads and proteins in pH 9.4 carbonate buffer overnight in the cold. The beads are then washed and stored in medium containing 1% BSA for up to 3 weeks at 4 °C

displacement is optically recorded using a microscope and an externally triggered CCD camera, and the images are stored on a second computer (No. 2) using IPLab. Connections and arrowheads indicate the direction of information flow. (B) Examples of bead displacements (top) measured during a dynamic force regimen driven by electric current waveforms (bottom) consisting of multiple ($n = 8$) subsecond (100 msec) force pulses interspersed with two periods of sinusoidal oscillations (1.0 Hz, 0.5 Hz, from left to right) and ending with a single period of prolonged force (10 sec). Two hundred milliampere corresponds to ~300-pN force. (C) Analysis of cellular mechanotransduction. Application of a high stress (>1 nN) to cell surface integrins via a bound RGD-coated magnetic bead (white arrow) using MPC (left, phase contrast image; black arrowhead indicates position of electromagnet tip) increases intracellular calcium within seconds, as detected using microfluorimetric ratio imaging with the calcium-sensitive dye, FURA-2, and shown in the time series of pseudocolored fluorescence images at the right (color bar indicates intracellular calcium concentrations in nM). [Modified from Overby *et al.* (2005) and Matthews *et al.* (2006) with permission.]

(Plopper and Ingber, 1993). Immediately before an experiment, cells are incubated with beads (~20 beads/cell) for 10 min and then washed three times with PBS to remove unbound beads. An electronic (Eppendorf) micromanipulator is then used to position the tip of the microneedle near surface receptor-bound magnetic beads, while viewing through an inverted microscope with a 20–100× objective lens (Eclipse TE2000E, Nikon) (Fig. 7A). Images of the beads are recorded using an externally triggered CCD camera (CoolSnap HQ, Roper Scientific) and imaging software (IPLab, Scanalytics, Fairfax, Virginia). A computer-controlled amplifier (Model SRL40–6, Sorensen, San Diego, California) is used to provide electric current to the electromagnetic microneedle. A desired voltage waveform is generated with the LabVIEW software (ver. 5.0, National Instruments, Austin, Texas) and sent to the control terminals of the amplifier. IPLab or MATLAB software (version 6, The MathWorks, Natick, Massachusetts) can be used for analyzing the image sequence, quantifying bead displacements, and temporally aligning bead displacements against force waveforms.

In most experiments, the needle tip is positioned to a predetermined height (~5–100 μm) and horizontal distance (~5–60 μm) from the magnetic bead prior to force application. These distances and the electrical current determine the magnitude of forces applied to the magnetic beads. The LabVIEW program simultaneously initiates the waveform to the electromagnet, actuates image acquisition by the CCD camera, and provides digital data acquisition. Centroids of beads (Fig. 7B) are analyzed to determine the bead displacement or viscoelastic creep response as a function of time.

Compared to an optical laser tweezer which may be used to only briefly (10–15 sec) trap single integrin-bound beads on the surface of cells (Choquet *et al.*, 1997), the magnetic needle can apply forces to beads for much longer periods of time. This is because the laser trap generates a very steep force gradient at its edges. When a cell adaptively reinforces its adhesions to the bead, it moves to the perimeter of the trap. If the trap is not displaced to accommodate this, the resistive force drops rapidly, allowing the bead to escape and the cell to readjust itself to a zero-force state (Choquet *et al.*, 1997). In contrast, forces can be applied to multiple beads for longer periods of time (minutes to days) using a magnetic needle, which generates a broad magnetic field gradient near the needle tip. Mechanical forces also can be maintained on the bead during and after adaptive cellular strengthening (Matthews *et al.*, 2006). In addition, the magnitude of force that can be applied using the optical trap is limited due to the risk of thermal injury to the cells by the laser at higher energy levels—even for laser wavelengths that might seem far from the absorption band of water or biomolecules. The magnetic needle, on the other hand, causes no damage to the cell even at proximity, allowing strong forces (up to 10 nN on 4.5-μm beads) to be applied. Finally, unlike the optical trap, MPC can easily apply brief pulses or cyclical force regimens (Fig. 7B) which can be used to estimate the local static and dynamic mechanical properties of the cell, and in particular, of bead-associated focal adhesions or other surface receptor–cytoskeleton linkages.

E. Applications of MPC

Using the permanent magnetic needle, we have shown that cells exhibit different types of mechanical adaptation responses when tensional forces are applied through beads bound to integrin receptors. The cells display an immediate viscoelastic response due to the local passive material properties of associated integrin–cytoskeleton linkages and recruited focal adhesion proteins (Matthews *et al.*, 2004b, 2006) that results in almost complete elastic recovery. They also exhibit an early adaptive behavior characterized by pulse-to-pulse attenuation in bead displacement in response to an oscillatory force regimen composed of short (3 sec) force pulses. A later form of adaptive cell stiffening is observed in response to sustained (>15 sec) static stresses, and a fourth type of adaptation is a large-scale repositioning response in which beads exposed to prolonged (>1 min) static stresses are retracted back by the cell against the applied force (Fig. 5F).

MPC also can be used to analyze the molecular biochemical basis of cell mechanical responses. For example, we found that the immediate viscoelastic response and early adaptation behavior are affected by dissipating cytoskeletal prestress whereas the later adaptive response to longer stresses is not (Matthews *et al.*, 2006). The large-scale repositioning of beads in response to prolonged stress is prevented by inhibition of myosin-based tension generation, and by blocking mechanosensitive ion channels. In addition, the large-scale repositioning response requires that integrins be chemically activated through occupancy of the RGD-binding site. Thus, MPC enabled us to demonstrate that cells use multiple distinct mechanisms to sense and respond to static and dynamic changes in the level of mechanical stress applied to cell surface integrin receptors.

MPC also was used in combination with calcium ratio imaging in cells loaded with the calcium-sensitive dye, FURA-2, to show that application of >1-nN forces to integrin-bound beads elicits a wave of calcium release within 2–5 sec after force application which can be blocked by treating cells with the stress-sensitive ion channel blocker gadolinium chloride (Matthews *et al.*, 2006). In more recent studies, we have been able to detect increases in calcium within <100 msec after force application. These findings obtained with MPC indicate that force application to integrins can activate stress-sensitive ion channels directly at the site of force application within the same focal adhesion. This method may be particularly useful for dissecting out the earliest steps involved in mechanotransduction across integrins.

IV. Discussion and Future Implications

The interplay between mechanics and chemistry that occurs inside the living cytoplasm has profound effects on cell behavior, and understanding the molecular biophysical basis of mechanotransduction represents a critically important challenge in biology. New insight into mechanotransduction has resulted from

interdisciplinary approaches that creatively and seamlessly combine tools and techniques across disciplines. As described in this chapter, we have developed various hybrid techniques that borrow approaches from magnetics and materials engineering, and integrated them with more conventional cell and molecular biological tools to meet this challenge.

Our methods for microfabricating culture substrates have led to new insights into the physical and molecular basis of cell fate switching, as well as potentially offering new approaches for engineering artificial tissues and creating novel cell–biomaterial interfaces. The magnetic cytometry methods have provided new insight into how cells behave mechanically, as well as which molecules are used by cells to sense mechanical signals and to convert them into a biochemical response.

A major challenge for the future of this field is to expand our knowledge of cellular mechanotransduction within the context of living tissues and organisms as opposed to studying isolated cells in Petri dishes (Ingber, 2006). For example, establishment of regional variations of cell and ECM mechanics over micrometer distances may be critical for control of normal morphogenesis, and when dysregulated, may lead to tissue disorganization and tumor formation (Huang and Ingber, 1999, 2005; Ingber, 2005; Ingber and Jamieson, 1985; Moore *et al.*, 2005; Nelson *et al.*, 2005; Paszek *et al.*, 2005). Thus, entirely new methods are needed to measure the mechanics of individual cells and molecules *in situ* within tissue, organs and whole living organisms. Our magnetic methods are particularly useful in this regard because they are not limited by optical transmission. MTC, for example, has already been adapted to measure mechanical properties of macrophages in the lungs of living human patients (Stahlhofen and Moller, 1992). However, we and others will still need to develop entirely new methods (or combine old) to develop ways to image, manipulate and probe ECM, cell and subcellular structures in real-time *in vivo* to fully understand how structure and function are fully integrated in living tissues. A first step in this process might involve refinements of some of the methods we described here so that they can be used in studies with organ explants, embryonic rudiments, or 3D cell cultures. This may be facilitated by the development of new microfabrication approaches that allow fine spatial control over ECM ligands, cytokines and living cells in 3D, while also providing mechanical, optical and electrochemical inputs and readouts of cell behavior at multiple size scales.

Development of new methods often opens entirely novel avenues of investigation, and this certainly has been true in the field of cellular mechanotransduction. However, the methods described here may also have uses beyond study of mechanobiology. The magnetic cytometry techniques could, for example, provide a way to create real-time cellular sensors that act as optical readouts of mechanical force in the future. In fact, we have already created living cellular switches that can be actuated magnetically using MPC and read out optically by creating gene reporter constructs driven by cAMP signals (Overby *et al.*, 2004) that are elicited by force application (Meyer *et al.*, 2000). The magnetic microbeads we used for MTC and MPC also can be coated with enzymes and placed in different magnetic field

configurations to create artificial ECMs (e.g., fibrin gels) with defined structure on the nanometer scale that might be useful for tissue-engineering applications (Alsberg *et al.*, 2006). Thus, the development of methods for analysis of cell mechanics and mechanotransduction may impact science and medicine in ways one might have never imagined.

References

Alenghat, F. J., Fabry, B., Tsai, K. Y., Goldmann, W. H., and Ingber, D. E. (2000). Analysis of cell mechanics in single vinculin-deficient cells using a magnetic tweezer. *Biochem. Biophys. Res. Commun.* **277,** 93–99.

Alsberg, E., Feinstein, E., Joy, M. P., Prentiss, M., and Ingber, D. E. (2006). Magnetically-guided self-assembly of fibrin matrices with ordered nanoscale structure for tissue engineering. *Tissue Eng.* **12,** 3247–3256.

Brangwynne, C. P., MacKintosh, F. C., Kumar, S., Geisse, N. A., Talbot, J., Mahadevan, L., Parker, K. K., Ingber, D. E., and Weitz, D. A. (2006). Microtubules can bear enhanced compressive loads in living cells because of lateral reinforcement. *J. Cell Biol.* **173,** 733–741.

Brock, A., Chang, E., Ho, C. C., LeDuc, P., Jiang, X., Whitesides, G. M., and Ingber, D. E. (2003). Geometric determinants of directional cell motility revealed using microcontact printing. *Langmuir* **19,** 1611–1617.

Chen, C. S., Alonso, J. L., Ostuni, E., Whitesides, G. M., and Ingber, D. E. (2003). Cell shape provides global control of focal adhesion assembly. *Biochem. Biophys. Res. Commun.* **307,** 355–361.

Chen, C. S., Mrksich, M., Huang, S., Whitesides, G. M., and Ingber, D. E. (1997). Geometric control of cell life and death. *Science* **276,** 1425–1428.

Chen, C. S., Mrksich, M., Huang, S., Whitesides, G. M., and Ingber, D. E. (1998). Micropatterned surfaces for control of cell shape, position, and function. *Biotechnol. Prog.* **14,** 356–363.

Chen, J., Fabry, B., Schiffrin, E. L., and Wang, N. (2001). Twisting integrin receptors increases endothelin-1 gene expression in endothelial cells. *Am. J. Physiol., Cell Physiol.* **280,** C1475–C1484.

Chicurel, M. E., Singer, R. H., Meyer, C. J., and Ingber, D. E. (1998). Integrin binding and mechanical tension induce movement of mRNA and ribosomes to focal adhesions. *Nature* **392,** 730–733.

Choquet, D., Felsenfeld, D. P., and Sheetz, M. P. (1997). Extracellular matrix rigidity causes strengthening of integrin-cytoskeleton linkages. *Cell* **88,** 39–48.

Coughlin, M. F., and Stamenovic, D. (1998). A tensegrity model of the cytoskeleton in spread and round cells. *J. Biomech. Eng.* **120,** 770–777.

Coughlin, M. F., and Stamenovic, D. (2003). A prestressed cable network model of the adherent cell cytoskeleton. *Biophys. J.* **84,** 1328–1336.

Dai, J., and Sheetz, M. P. (1995). Mechanical properties of neuronal growth cone membranes studied by tether formation with laser optical tweezers. *Biophys. J.* **68,** 988–996.

Dike, L. E., Chen, C. S., Mrksich, M., Tien, J., Whitesides, G. M., and Ingber, D. E. (1999). Geometric control of switching between growth, apoptosis, and differentiation during angiogenesis using micropatterned substrates. *In Vitro Cell. Dev. Biol. Anim.* **35,** 441–448.

Dong, C. S. R., and Sung, K. L. (1991). Cytoplasmic rheology of passive neutrophils. *Biorheology* **28,** 557–567.

Fabry, B., Maksym, G. N., Shore, S. A., Moore, P. E., Panettieri, R. A., Jr, Butler, J. P., and Fredberg, J. J. (2001). Selected contribution: Time course and heterogeneity of contractile responses in cultured human airway smooth muscle cells. *J. Appl. Physiol.* **91,** 986–994.

Hu, S., Eberhard, L., Chen, J., Love, J. C., Butler, J. P., Fredberg, J. J., Whitesides, G. M., and Wang, N. (2004). Mechanical anisotropy of adherent cells probed by a three-dimensional magnetic twisting device. *Am. J. Physiol., Cell Physiol.* **287,** C1184–C1191.

Hu, S. H., Chen, J., Fabry, B., Numaguchi, Y., Gouldstone, A., Ingber, D. E., Fredberg, J. J., Butler, J. P., and Wang, N. (2003). Intracellular stress tomography reveals stress focusing and structural anisotropy in cytoskeleton of living cells. *Am. J. Physiol., Cell Physiol.* **285,** C1082–C1090.

Huang, S., and Ingber, D. E. (1999). The structural and mechanical complexity of cell-growth control. *Nat. Cell Biol.* **1,** E131–E138.

Huang, S., and Ingber, D. E. (2005). Cell tension, matrix mechanics, and cancer development. *Cancer Cell* **8,** 175–176.

Ingber, D. E. (1990). Fibronectin controls capillary endothelial cell growth by modulating cell shape. *Proc. Natl. Acad. Sci. USA* **87,** 3579–3583.

Ingber, D. E. (1991). Integrins as mechanochemical transducers. *Curr. Opin. Cell Biol.* **3,** 841–848.

Ingber, D. E. (1993a). Cellular tensegrity: Defining new rules of biological design that govern the cytoskeleton. *J. Cell Sci.* **104**(Pt. 3), 613–627.

Ingber, D. E. (1993b). The riddle of morphogenesis: A question of solution chemistry or molecular cell engineering? *Cell* **75,** 1249–1252.

Ingber, D. E. (1997). Integrins, tensegrity, and mechanotransduction. *Gravit. Space Biol. Bull.* **10,** 49–55.

Ingber, D. E. (2003a). Mechanobiology and diseases of mechanotransduction. *Ann. Med.* **35,** 564–577.

Ingber, D. E. (2003b). Tensegrity II. How structural networks influence cellular information processing networks. *J. Cell Sci.* **116,** 1397–1408.

Ingber, D. E. (2005). Mechanical control of tissue growth: Function follows form. *Proc. Natl. Acad. Sci. USA* **102,** 11571–11572.

Ingber, D. E. (2006). Cellular mechanotransduction: Putting all the pieces together again. *FASEB J.* **20,** 811–827.

Ingber, D. E., and Folkman, J. (1989a). How does extracellular matrix control capillary morphogenesis? *Cell* **58,** 803–805.

Ingber, D. E., and Folkman, J. (1989b). Mechanochemical switching between growth and differentiation during fibroblast growth factor-stimulated angiogenesis *in vitro*: Role of extracellular matrix. *J. Cell Biol.* **109,** 317–330.

Ingber, D. E., and Jamieson, J. D. (1985). Cells as tensegrity structures: Architectural regulation of histodifferentiation by physical forces transduced over basement membrane. *In* "Gene Expression During Normal and Malignant Differentiation" (L. C. Andersson, C. G. Gahmberg, and P. Ekblom, eds.), pp. 13–32. Academic Press, Orlando.

Jiang, X., Bruzewicz, D. A., Wong, A. P., Piel, M., and Whitesides, G. M. (2005). Directing cell migration with asymmetric micropatterns. *Proc. Natl. Acad. Sci. USA* **102,** 975–978.

Kato, M., and Mrksich, M. (2004). Using model substrates to study the dependence of focal adhesion formation on the affinity of integrin-ligand complexes. *Biochemistry* **43,** 2699–2707.

Kumar, S., Maxwell, I. Z., Heisterkamp, A., Polte, T. R., Lele, T. P., Salanga, M., Mazur, E., and Ingber, D. E. (2006). Viscoelastic retraction of single living stress fibers and its impact on cell shape, cytoskeletal organization, and extracellular matrix mechanics. *Biophys. J.* **90,** 3762–3773.

Laurent, V. M., Canadas, P., Fodil, R., Planus, E., Asnacios, A., Wendling, S., and Isabey, D. (2002). Tensegrity behaviour of cortical and cytosolic cytoskeletal components in twisted living adherent cells. *Acta Biotheor.* **50,** 331–356.

Lele, T. P., Pendse, J., Kumar, S., Salanga, M., Karavitis, J., and Ingber, D. E. (2006). Mechanical forces alter zyxin unbinding kinetics within focal adhesions of living cells. *J. Cell. Physiol.* **207,** 187–194.

Maniotis, A. J., Chen, C. S., and Ingber, D. E. (1997). Demonstration of mechanical connections between integrins, cytoskeletal filaments, and nucleoplasm that stabilize nuclear structure. *Proc. Natl. Acad. Sci. USA* **94,** 849–854.

Matthews, B. D., LaVan, D. A., Overby, D. R., Karavitis, J., and Ingber, D. E. (2004a). Electromagnetic needles with submicron pole tip radii for nanomanipulation of biomolecules and living cells. *Appl. Phys. Lett.* **85,** 2968–2970.

Matthews, B. D., Overby, D. R., Alenghat, F. J., Karavitis, J., Numaguchi, Y., Allen, P. G., and Ingber, D. E. (2004b). Mechanical properties of individual focal adhesions probed with a magnetic microneedle. *Biochem. Biophys. Res. Commun.* **313,** 758–764.

Matthews, B. D., Overby, D. R., Mannix, R., and Ingber, D. E. (2006). Cellular adaptation to mechanical stress: Role of integrins, Rho, cytoskeletal tension, and mechanosensitive ion channels. *J. Cell. Sci.* **119**(Pt. 3), 508–518.

Meyer, C. J., Alenghat, F. J., Rim, P., Fong, J. H., Fabry, B., and Ingber, D. E. (2000). Mechanical control of cyclic AMP signalling and gene transcription through integrins. *Nat. Cell Biol.* **2,** 666–668.

Mooney, D., Hansen, L., Vacanti, J., Langer, R., Farmer, S., and Ingber, D. (1992). Switching from differentiation to growth in hepatocytes: Control by extracellular matrix. *J. Cell. Physiol.* **151,** 497–505.

Moore, K. A., Polte, T., Huang, S., Shi, B., Alsberg, E., Sunday, M. E., and Ingber, D. E. (2005). Control of basement membrane remodeling and epithelial branching morphogenesis in embryonic lung by Rho and cytoskeletal tension. *Dev. Dyn.* **232,** 268–281.

Nelson, C. M., Jean, R. P., Tan, J. L., Liu, W. F., Sniadecki, N. J., Spector, A. A., and Chen, C. S. (2005). Emergent patterns of growth controlled by multicellular form and mechanics. *Proc. Natl. Acad. Sci. USA* **102,** 11594–11599.

Overby, D. R., Alenghat, F. J., Montoya-Zavala, M., Bei, H. C., Oh, P., Karavitis, J., and Ingber, D. E. (2004). Magnetic cellular switches. *IEEE Trans. Magn.* **40,** 2958–2960.

Overby, D. R., Matthews, B. D., Alsberg, E., and Ingber, D. E. (2005). Novel dynamic rheological behavior of focal adhesions measured within single cells using electromagnetic pulling cytometry. *Acta Biomater.* **1,** 295–303.

Parker, K. K., Brock, A. L., Brangwynne, C., Mannix, R. J., Wang, N., Ostuni, E., Geisse, N. A., Adams, J. C., Whitesides, G. M., and Ingber, D. E. (2002). Directional control of lamellipodia extension by constraining cell shape and orienting cell tractional forces. *FASEB J.* **16,** 1195–1204.

Paszek, M. J., Zahir, N., Johnson, K. R., Lakins, J. N., Rozenberg, G. I., Gefen, A., Reinhart-King, C. A., Margulies, S. S., Dembo, M., Boettiger, D., Hammer, D. A., and Weaver, V. M. (2005). Tensional homeostasis and the malignant phenotype. *Cancer Cell* **8,** 241–254.

Pelham, R. J., Jr., and Wang, Y. (1997). Cell locomotion and focal adhesions are regulated by substrate flexibility. *Proc. Natl. Acad. Sci. USA* **94,** 13661–13665.

Plopper, G., and Ingber, D. E. (1993). Rapid induction and isolation of focal adhesion complexes. *Biochem. Biophys. Res. Commun.* **193,** 571–578.

Polte, T. R., Eichler, G. S., Wang, N., and Ingber, D. E. (2004). Extracellular matrix controls myosin light chain phosphorylation and cell contractility through modulation of cell shape and cytoskeletal prestress. *Am. J. Physiol., Cell Physiol.* **286,** C518–C528.

Potard, U. S., Butler, J. P., and Wang, N. (1997). Cytoskeletal mechanics in confluent epithelial cells probed through integrins and E-cadherins. *Am. J. Physiol.* **272,** C1654–C1663.

Prime, K. L., and Whitesides, G. M. (1991). Self-assembled organic monolayers: Model systems for studying adsorption of proteins at surfaces. *Science* **252,** 1164–1167.

Roberts, C., Chen, C., Mrksich, M., Martichonok, V., Ingber, D., and Whitesides, G. M. (1998). Using mixed self-assembled monolayers presenting RGD and (EG)(3)OH groups to characterize long-term attachment of bovine capillary endothelial cells to surfaces. *J. Am. Chem. Soc.* **120,** 6548–6555.

Rogers, J. A., Paul, K. E., and Whitesides, G. M. (1998). Quantifying distortions in soft lithography. *J. Vac. Sci. Technol. B* **16,** 88–97.

Ryan, D., Parviz, B. A., Linder, V., Semetey, V., Sia, S. K., Su, J., Mrksich, M., and Whitesides, G. M. (2004). Patterning multiple aligned self-assembled monolayers using light. *Langmuir* **20,** 9080–9088.

Schwartz, M. A., Lechene, C., and Ingber, D. E. (1991). Insoluble fibronectin activates the Na/H antiporter by clustering and immobilizing integrin alpha 5 beta 1, independent of cell shape. *Proc. Natl. Acad. Sci. USA* **88,** 7849–7853.

Shroff, S. G., Saner, D. R., and Lal, R. (1995). Dynamic micromechanical properties of cultured rat atrial myocytes measured by atomic force microscopy. *Am. J. Physiol.* **269,** C286–C292.

Singhvi, R., Kumar, A., Lopez, G. P., Stephanopoulos, G. N., Wang, D. I., Whitesides, G. M., and Ingber, D. E. (1994). Engineering cell shape and function. *Science* **264,** 696–698.

Stahlhofen, W., and Moller, W. (1992). Investigation of the defense system of the human lungs with ferrimagnetic particles. *J. Aerosol Med.* **5,** 221–228.

Stamenovic, D., and Coughlin, M. F. (2000). A quantitative model of cellular elasticity based on tensegrity. *J. Biomech. Eng.* **122,** 39–43.

Stamenovic, D., Fredberg, J. J., Wang, N., Butler, J. P., and Ingber, D. E. (1996). A microstructural approach to cytoskeletal mechanics based on tensegrity. *J. Theor. Biol.* **181,** 125–136.

Tagawa, H., Wang, N., Narishige, T., Ingber, D. E., Zile, M. R., and Cooper, G., 4th. (1997). Cytoskeletal mechanics in pressure-overload cardiac hypertropy. *Circ. Res.* **80**(2), 295–296.

Tan, J. L., Liu, W., Nelson, C. M., Raghavan, S., and Chen, C. S. (2004). Simple approach to micropattern cells on common culture substrates by tuning substrate wettability. *Tissue Eng.* **10,** 865–872.

Valberg, P. A., and Butler, J. P. (1987). Magnetic particle motions within living cells. Physical theory and techniques. *Biophys. J.* **52,** 537–550.

Wang, N., Butler, J. P., and Ingber, D. E. (1993). Mechanotransduction across the cell surface and through the cytoskeleton. *Science* **260,** 1124–1127.

Wang, N., and Ingber, D. E. (1994). Control of cytoskeletal mechanics by extracellular matrix, cell shape, and mechanical tension. *Biophys. J.* **66,** 2181–2189.

Wang, N., and Ingber, D. E. (1995). Probing transmembrane mechanical coupling and cytomechanics using magnetic twisting cytometry. *Biochem. Cell Biol.* **73,** 327–335.

Wang, N., Ostuni, E., Whitesides, G. M., and Ingber, D. E. (2002a). Micropatterning tractional forces in living cells. *Cell Motil. Cytoskeleton* **52,** 97–106.

Wang, N., Tolic-Norrelykke, I. M., Chen, J., Mijailovich, S. M., Butler, J. P., Fredberg, J. J., and Stamenovic, D. (2002b). Cell prestress. I. Stiffness and prestress are closely associated in adherent contractile cells. *Am. J. Physiol., Cell Physiol.* **282,** C606–C616.

Wang, Y. L., and Pelham, R. J., Jr (1998). Preparation of a flexible, porous polyacrylamide substrate for mechanical studies of cultured cells. *Methods Enzymol.* **298,** 489–496.

Whitesides, G. M., Ostuni, E., Takayama, S., Jiang, X., and Ingber, D. E. (2001). Soft lithography in biology and biochemistry. *Annu. Rev. Biomed. Eng.* **3,** 335–373.

Xia, Y., and Whitesides, G. M. (1998). Soft lithography. *Angew. Chem. Int. Ed. Engl.* **37,** 550–575.

Yeo, W. S., Hodneland, C. D., and Mrksich, M. (2001). Electroactive monolayer substrates that selectively release adherent cells. *Chembiochem* **2,** 590–593.

Yeo, W. S., Yousaf, M. N., and Mrksich, M. (2003). Dynamic interfaces between cells and surfaces: Electroactive substrates that sequentially release and attach cells. *J. Am. Chem. Soc.* **125,** 14994–14995.

Yoshida, M., Westlin, W. F., Wang, N., Ingber, D. E., Rosenzweig, A., Resnick, N., and Gimbrone, M. A., Jr. (1996). Leukocyte adhesion to vascular endothelium induces E-selectin linkage to the actin cytoskeleton. *J. Cell Biol.* **133,** 445–455.

Yousaf, M. N., Houseman, B. T., and Mrksich, M. (2001). Using electroactive substrates to pattern the attachment of two different cell populations. *Proc. Natl. Acad. Sci. USA* **98,** 5992–5996.